Contents lists available at ScienceDirect

Archives of Biochemistry and Biophysics

Structure and dynamics of the cyanobacterial regulator SipA

José L. Neira [a,b,*], María Luisa López-Redondo [c], Ana Cámara-Artigas [d], Alberto Marina [e], Asunción Contreras [f]

[a] *IDIBE, Universidad Miguel Hernández, 03202, Elche, Alicante, Spain*
[b] *Instituto de Biocomputación y Física de Sistemas Complejos (BIFI), Universidad de Zaragoza, 50018, Zaragoza, Spain*
[c] *Unidad Regulación de La Síntesis de Proteínas, Instituto de Biomedicina de Valencia (CSIC), 46010, Valencia, Spain*
[d] *Departamento de Química y Física, Research Center CIAIMBITAL, Universidad de Almería- CeiA3, 04120, Almería, Spain*
[e] *Instituto de Biomedicina de Valencia (CSIC) y Centro de Investigación Biomédica en Red en Enfermedades Raras (CIBERER), 46010, Valencia, Spain*
[f] *División de Genética, Universidad de Alicante, 03080, Alicante, Spain*

ARTICLE INFO

ABSTRACT

The small, 78-residue long, regulator SipA interacts with the non-bleaching sensor histidine kinase (NblS). We have solved the solution structure of SipA on the basis of 990 nuclear Overhauser effect- (NOE-) derived distance constraints. The average pairwise root-mean-square deviation (RMSD) for the twenty best structures for the backbone residues, obtained by CYANA, was 1.35 ± 0.21 Å, and 1.90 ± 0.16 Å when all heavy atoms were considered (the target function of CYANA was 0.540 ± 0.08). The structure is that of a β-II class protein, basically formed by a five-stranded β-sheet composed of antiparallel strands following the arrangement: Gly6-Leu11 (β-strand 1), which packs against Leu66-Val69 (β-strand 5) on one side, and against Gly36-Thr42 (β-strand 2) on the other side; Trp50-Phe54 (β-strand 3); and Gly57-Leu60 (β-strand 4). The protein is highly mobile, as shown by measurements of R_1, R_2, NOE and η_{xy} relaxation parameters, with an average order parameter ($<S^2>$) of 0.70; this mobility encompasses movements in different time scales. We hypothesize that this high flexibility allows the interaction with other proteins (among them NblS), and it explains the large conformational stability of SipA.

1. Introduction

Small proteins appear to play critical roles in key cyanobacterial processes such photosynthesis or regulation of the carbon-to-nitrogen balance [1–3]. One of these, SipA (non-bleaching sensor (NblS) histidine kinase (HK) interacting protein A) is a 78-residue-long protein, which is a unique and conserved cyanobacterial protein identified by its ability to bind to the HK domain of NblS [4,5]. The interaction with NblS is, so far, the sole function described for SipA.

SipA stimulates the auto-kinase activity of NblS [6], a protein which is essential for cyanobacterial survival [7], and one of the few HKs widely conserved in cyanobacteria [8]. NblS, *via* its also essential response regulator RpaB [7,9], controls multiple processes in response to a variety of environmental conditions [9–11]. However, the signals and molecular details involved in the regulation of NblS by SipA remain elusive.

Structures of the complexes between HKs and their regulators, or even those of the isolated regulators, give important insights into the phosphorylation transfer steps and the signal transduction mechanisms in two-component systems [12]. Therefore, determination of SipA structure and its molecular features are required to understand the biological meaning of the NblS-SipA regulatory interaction, as well as to further increase: (i) the structural coverage of the protein universe; and, (ii) our knowledge on the emerging field of cyanobacterial small regulators.

We have previously shown that SipA from *Synechococcus* sp PCC 7942 is a highly stable protein [13] in a wide pH range. With the fluorescence and far-ultraviolet (far-UV) circular dichroism (CD) findings, we have set the conditions to carry out NMR studies to allow for its assignment and the elucidation of SipA three-dimensional structure. In this work, we report the NMR assignment, the 3D-structure in solution and the dynamics of SipA in the range of picosecond-to-nanoseconds. The structure is formed by a five-stranded β-sheet composed of antiparallel strands following the arrangement: Gly6-Leu11 (β-strand 1), which packs against Leu66-Val69 (β-strand 5) on one side, and against Gly36-Thr42 (β-strand 2) on the other; Trp50-Phe54 (β-strand 3); and Gly57-Leu60 (β-strand 4). The dynamics indicate that the protein had a

high flexibility in the picoseconds-to-nanoseconds time regime. The high mobility does not only affect the loops connecting the strands, but also the elements of secondary structure. We hypothesize that this high dynamics in such time range allows for interactions with other proteins, such as NblS and explain the unsuccessful attempts to find conditions of protein crystallization (MLL-R and AM, unpublished results). Moreover, the high mobility explains the high thermal conformational stability by an entropic effect.

2. Materials and methods

2.1. Materials

Imidazole, Trizma base, DNase, SIGMAFAST protease tablets, deuterium oxide (99 % atom % in ^{2}H$_2$O), NaCl, Ni^{2+}-resin, 3-(trimethylsilyl) propionic acid-2,2,3,3-^{2}H$_4$-sodium salt (TSP) and Amicon centrifugal devices with a molecular weight cut-off of 3 kDa were from Sigma (Madrid, Spain). The β-mercaptoethanol was from BioRad (Madrid, Spain). Kanamycin and isopropyl-β-D-1-thiogalactopyranoside (IPTG) were obtained from Apollo Scientific (Stockport, UK). Triton X-100, dialysis tubing with a molecular weight cut-off of 3500 Da and the SDS protein marker (PAGEmark Tricolor) were from VWR (Barcelona, Spain). The rest of the materials were of analytical grade. Water was deionized and purified on a Millipore system.

The maltose-TEV (tobacco etch virus) protease was requested from the Harvard depository of clones (http://plasmid.med.harvard.edu /PLASMID/) and expressed and purified as described [14].

2.2. SipA expression and purification

The protein expression in rich media and removal of the His-tag has been described before [5,13]. The TEV cleavage sequence is formed by –ENLYFQG–, where the protease cleaves between the Q and G residues. After cleavage with the in-home-produced TEV protease, the resulting protein had the GAM– sequence at its N terminus. The expression in M9 minimal media was supplemented with 1 g/L of ^{15}NH$_4$Cl for ^{15}N-labelled samples, or, alternatively for double (^{13}C, ^{15}N)-labelled samples used in SipA assignment, with 1 g/L of ^{15}NH$_4$Cl and 2 g/L of ^{13}C-glucose. The addition of 1 mM IPTG (final concentration in 1 L of media), when absorbance of the culture at 600 nm was 0.8–1.0, induced protein expression either in LB or in M9 minimal media. After adding IPTG, the cells were incubated for 3 h at 37 °C and harvested by

centrifugation at 20,000 rpm at 5 °C. The rest of the purification steps are the same as in rich media [5,13].

Protein concentration was determined from the extinction coefficient of model compounds [15].

2.3. Nuclear magnetic resonance (NMR)

NMR samples for homonuclear experiments were prepared by concentrating and exchanging the solution containing SipA in Amicon 3 K centrifugal devices, in a final 9:1H$_2$O:^{2}H$_2$O solution, with a 0.02 % NaN$_3$ in acetate buffer (50 mM), pH 5.5. The solution was centrifuged briefly to remove insoluble protein and then transferred to a 5 mm NMR tube. Spectra were recorded on a Bruker Avance 500 MHz spectrometer (Bruker GmbH, Karlsruhe, Germany), with z-pulse field gradients and a TXI probe, equipped with Topspin 2.1 software (Bruker, Karlsruhe, Germany). Experiments were acquired at 25 °C; the temperature of the probe was calibrated with methanol, as described [16]. The pH of the solution was measured at the beginning and end of the complete series of NMR experiments by using a Russell glass electrode, without finding any difference between both measurements. Measurements of the pH reported here represent apparent pH values, without correction for isotope effects. TSP was used as the internal chemical shift reference, and the values of the chemical shifts of its protons were corrected for the pH value of the sample [16].

The NMR experiments with ^{13}C/^{15}N-SipA were performed in the same magnet with the same buffer, and at the same temperature as the homonuclear experiments. Protein concentration was 2.5 mM for either double-labelled or un-labelled samples.

(a) *Assignment of SipA*: The NMR experiments used for sequence specific assignment of HN, N, C$_\alpha$ and C$_\beta$ resonances of a^{13}C/^{15}N-SipA were HNCACB, HNCA, HNCO, HBHACONH and HCCCONH [16]. 3D NOESY-HSQC (mixing time 125 ms) and TOCSY-HSQC (mixing time, 80 ms) spectra were also acquired to allow for identification of additional protons in the side-chains of residues, and to find NOE restrictions. The 2D homonuclear NOESY and TOCSY experiments were also acquired to complete the assignment of the experiments described above, with the same mixing time described above for the 3D variants. The 2D experiments aimed to identify the amino acid type were also acquired [17,18]. The details of the acquisition parameters of all the experiments used for assignment of the protein and structural elucidation are shown in Supplementary Table 1 (Table ST1). The chemical shifts have been deposited in the BMRB (Biomagnetic Resonance Bank) with number 52171. The 2D^{15}N-HSQC spectra were also acquired at the beginning, middle and the end of the triple-resonance suite of experiments to ensure sample integrity. The ^{13}C and ^{15}N nuclei were indirectly referenced, with respect to TSP, considering the pH-dependence of its resonances [16]. Processing and analysis of data were carried out by using Topspin 2.1 working on a PC.

(b) *Relaxation measurements of SipA:* Experiments were acquired with an ^{15}N-labelled sample of SipA. We acquired ^{15}N–R_1, ^{15}N–R_2, ^{1}H–^{15}N NOE and the transverse η$_{xy}$ (^{1}H–^{15}N dipolar/^{15}N chemical shift anisotropy, CSA) cross-correlation experiments. All the relaxation measurements were determined in an interleaved manner to ensure that the experimental conditions were the same for the different relaxation delays. The temperature was the same used in the assignment (25 °C). All experiments were acquired by using gradient pulse sequences developed by Kay and co-workers [19]. The T_1 ($=1/R_1$) relaxation time was measured with typically 10 inversion-recovery delays, varying from 5 to 750 ms; T_2 ($=1/R_2$) was determined by collecting 8 time points ranging from 50 to 400 ms. Two relaxation delays were randomly repeated in each series of rates to ensure reproducibility. For the T_1 and T_2 pulse sequences, the delay between scans was 5 s. The spectra were zero-filled in the F$_1$ dimension two times, and processed by

using the same shifted square sine window function, through all the T_1 and T_2 experiments. Cross-peaks intensities at each time were measured by integration of signals by using Topspin 2.1. Intensity variation was fitted to simple exponential functions, with a pre-exponential factor by using KaleidaGraph (Adelbeck software). Indicated errors in the T_1 and T_2 were from fitting.

The ^{1}H–^{15}N NOE experiment was measured by recording interleaved spectra with or without proton saturation. The ^{1}H–^{15}N NOE spectrum recorded in the presence of proton saturation was acquired with a saturation time of 8 s (achieved by a series of $120°$ pulses separated by 5 ms delays). The ^{1}H–^{15}N NOE spectrum recorded without proton saturation incorporated a relaxation delay of 8 s. The ^{1}H–^{15}N NOE experiment (with and without saturation) was repeated twice. The NOE ratio was defined as NOE $= I_{sat}/I_{ref}$, where I_{sat} is the intensity of the corresponding cross-peak in the saturated spectrum and I_{ref} is that in the reference (non-saturated) spectrum. Both intensities were measured by using Topspin 2.1. The two spectra were zero-filled in the F_1 dimension two times, and processed by using the same shifted square sine window function. The errors in the determined NOEs were estimated to be 10%, as judged from the integrated regions where no peaks were observed.

All spectra for the measurement of ^{15}N–R_1, ^{15}N–R_2 and ^{1}H–^{15}N NOE were recorded with 2048 × 180 complex matrices in the F_2 and F_1 dimensions, respectively, with typically 32 scans (NOE experiment) and 16 scans (R_1 and R_2 experiments) *per* F_1 experiment. Spectral widths of 1935 and 7000 Hz were used in F_1 and F_2, respectively; the ^{15}N carrier was set at 115 ppm and that of ^{1}H was set on the water signal in all the experiments.

The transverse, η_{xy} (^{1}H–^{15}N dipolar/^{15}N chemical shift anisotropy, CSA), cross-correlation rate constants were measured with spectral widths of 1800 and 7000 Hz in F_1 and F_2, respectively, and the ^{15}N carrier was set at 115 ppm and that of ^{1}H was set on the water signal in all the experiments. One set of cross-relaxation (which leads to I_{cross}) and auto-relaxation (which yields I_{auto}) experiments were acquired for each of the relaxation delays. Both sets of experiments consisted of 256 experiments in the F_1 dimension and 2 K data points in the F_2 dimension; 32 scans were acquired *per* F_1 experiment. The relaxation delays, T, were 13, 18, 22, 26, and 31 ms. Control experiments (acquiring the two experiments *per* relaxation time) were acquired with 64 scans and relaxation delays of 18, 22, 26, and 31 ms. All the spectra were zero-filled in the F_1 dimension two times and processed by using the same shifted sine square window function for each relaxation time. The peak intensities were measured by using Topspin 2.1. Errors in the intensities were determined from the pairwise root-mean-square deviations obtained by repeating experiments at two selected times. The η_{xy} was derived from the one-parameter fitting equation: $I_{cross}/I_{auto} = \tanh(\eta_{xy}T)$, where T is the corresponding relaxation delay described above. The ratios of I_{cross}/I_{auto} were fitted to such equation by using Kaleidagraph. The values of the η_{xy} were similar, within the experimental error, in both the current (32 scans in the F_1 dimension) and control (64 scans in the F_1 dimension) experiments.

The experimentally measured transverse relaxation rate, R_2 ($R_2 = 1/T_2$), can be expressed by:

$$R_2 = R_2^0 + R_{ex} \tag{1}$$

where R_{ex} is the contribution to the transverse relaxation rate caused by conformational processes (millisecond-to-millisecond); and R_2^0 is the transverse relaxation rate, which does not contain any influence from those slow movements. Then, to quantify the microsecond-to-millisecond dynamics, it is necessary to obtain the R_2^0 independently. The R_2^0 is obtained from the experimental value of η_{xy} [20,21]:

$$R_2^0 = 1.2589\,\eta_{xy} + 1.3[(NOE - 1)R_1]\frac{\gamma_N}{\gamma_H} \tag{2}$$

where the NOE value has been described above, and γ_N and γ_H are the gyromagnetic rations of ^{15}N and ^{1}H, respectively (-2.712×10^7 rad T^{-1} s^{-1} and 26.75×10^7 rad T^{-1} s^{-1}).

2.4. Structure calculations

All spectra were analyzed by using the Sparky software [22]. After integration, the peak volumes of the NOESY spectra and the chemical shifts list were output to a CYANA-compatible format [23–25]. The automatic calibration method implemented in CYANA, CALIBA [25], was run to transform the peak volumes into distances. Default weighting factors were attributed to the different restraint categories for different types of atoms. The upper limits obtained were used without modification for the initial structure calculations.

Structures of SipA were calculated by using the NOE distance restraints with CYANA. At subsequent steps during the calculation of the structures, those distance restraints were combined in an iterative fashion with: (i) backbone φ and ψ angle restraints as predicted by TALOS + [26] based on the chemical shifts of C_α, C_β, H_α, H_β, NH, the amide N and CO atoms (only when angular predictions were classified as "good" were used in the calculations); and, (ii) hydrogen-bonds obtained from the remaining amide protons of SipA observed in hydrogen-exchange experiments carried out by dissolving the protein in 99.99 % D$_2$O, at 2.5 mM final concentration, and acquiring a 4-h long 2D ^{1}H–^{15}N HSQC NMR spectrum. The introduced restraints of hydrogen-bonds were in all cases well-suited with the observed, experimental distance restraints from NOESY spectra, and they were only introduced as restraints, when the first runs of CYANA, predicted them in at least 5 of the best 20 conformers (with the lowest CYANA target functions). Each hydrogen-bond was specified by two distance restraints: HN–O distance of 1.7–2.3 Å and N–O distance of 2.4–3.3 Å.

The resulting initial conformers with the lowest values of the target function were used: (i) to assign additional, ambiguous peaks in the NOESY spectrum, which had not been previously used as restraints; and (ii) to introduce new hydrogen-bonds. The cycle of calculations and assignments was repeated until no further assignments were possible. The quality of the introduced constraints was checked at every step by analyzing the restraint violations of the calculated conformers, as calculated from CYANA. The NOE cross-peaks corresponding to restraints that were consistently violated in a significant number of structures were checked for possible overlap in the NOESY spectra and the corresponding restraints were modified. The cycle was repeated until no consistent violation was detected.

In the final calculation, a total of 400 random conformers were annealed in 12,000 steps. The 20 conformers with the lowest CYANA target function constituted the final family of structures of SipA. The quality of the structures was evaluated in terms of deviations from ideal bond lengths, angles, and through Ramachandran plots by using the PSVS server [27].

2.5. AlphaFold model of SipA

The sequence of SipA was introduced in the *phenix.predit_model* interface in Phenix [28] to generate a computational AlphaFold model (AF_model). The best model containing residues 1 to 76 of the SipA sequence was improved by using the *phenix.process_predicted_model* interface, and residues with low predicted local distance difference test score (plDDT) values were removed. The final best AF_model contains residues Asp2-Asp22 and Met26-Glu70.

3. Results

3.1. Description of the structure of SipA

We carried out the assignment of SipA by using triple resonance experiments. Except for the amide proton, HN, of Ser76, all the ^{15}N, ^{1}H$_\alpha$ and HN of the backbone residues were fully assigned. The assignment of

the ^{1}H chemical shifts of the side chains of all residues was complete at a 98 %. The assignment for the ^{13}CO, ^{13}C$_\alpha$ and ^{13}C$_\beta$ was complete in a 95 % (BMRB 52171).

Several repeated rounds of ambiguous long-range and non-sequential NOEs were assigned and converted to distance constraints to be used as input data in CYANA. Table 1 summarizes the number of structurally relevant intra-residual, sequential, and medium- and long-range constraints used in the final round of calculations (Fig. 1). The average pairwise root-mean-square deviation (RMSD) values for all backbone atoms and heavy atoms between residues Ile5 and Glu70 were 1.35 ± 0.21 (1.11–1.86) Å and 1.90 ± 0.16 (1.65–2.32) Å, respectively. When only the residues ordered (i.e., the β-strands) are considered in the calculation of the RMSD, the values are 0.4 Å and 0.9 Å, for all the backbone and heavy atoms, respectively, as calculated from the PSVS web-server [27]. The target function of CYANA had an average value of 0.540 ± 0.008 (0.44–0.65) (Fig. 1 A). The RMSD for covalent bonds relative to the standard value was 0.001 Å, and that for covalent angles was 0.2°, as indicated by the PSVS web-server [27]. From the statistics in Table 1 and it can be seen that the percentage of residues in the most favored region of the Ramachandran plot is 42 %; we think that this is due to the presence of the long loops and disordered regions of the protein, which have a high mobility and where there are no a high number of long-distant NOEs. In fact, careful examination of the PDB validation reports indicates that when only the residues in β-strands are considered, most of them are in the most favored region of the Ramachandran plot. This conclusion was not surprising, as when only those ordered residues were considered for the calculation, the RMSDs for the backbone and heavy atoms were smaller (see above in this paragraph). Furthermore, the RMSDs *per* residue for each of the twenty NMR structures were also calculated and they were also lower in the β-strands (see below Fig. 5 C).

The overall fold of SipA shows a five-stranded β-sheet, arranged in an anti-parallel manner (Fig. 1): Gly6-Leu11 (β-strand 1), which packs against Leu66-Val69 (β-strand 5) on one side, and against Gly36-Thr42 (β-strand 2) on the other; Trp50-Phe54 (β-strand 3); and Gly57-Leu60 (β-strand 4). The strands are connected by long loops, which are mainly disordered, or two β-turns type II: Leu44-Gly47 (between β-strands 2 and 3); and Phe54-Gly57 (between β-strands 3 and 4), as indicated by VADAR [29]. The use of the chemical shifts of ^{13}C$_\alpha$, ^{13}C$_\beta$,

Table 1
NMR restraints and structural statistics for the best 20 structures of SipA.

Restraints	
Total number of restraints	
NOE restraints[a]	990
Intra-residue (i-j = 0)	271
Sequential (|i-j| = 1)	272
Medium-range (|i-j| ≤ 4)	221
Long-range (|i-j| ≥ 4)	226
Dihedral angle restraints	50 (for φ and ψ angles)
Hydrogen-bond restraints	13 × 2[b]
RMSD from the mean structure residues Ile5-Glu70	
Average backbone	1.35 ± 0.21 Å
Heavy atoms	1.90 ± 0.16 Å
Bond angles[c]	0.2°
Bond lengths[c]	0.001 Å
Number of close contacts[c,d]	0
Ramachandran summary for all residues in the 20 conformers from Procheck (in %)[c]	
Most favored	42.1
Additionally allowed regions	35.2
Generously allowed regions	17.3
Disallowed regions	5.4

[a] The i and j represent two residues of the sequence of SipA.

[b] For each hydrogen-bond two restrictions were introduced: the HN–O and the N–O distances.

[c] Obtained from PSVS server [27].

[d] The number of close contacts is within 1.6 Å for hydrogen atoms, and 2.2 Å for heavy atoms, according to the PSVS server [27].

^{13}CO, H$_\alpha$, H$_\beta$, NH and amide ^{15}N atoms in TALOS + server [26] also predicted the five-stranded pleated, twisted β-sheet: Arg8-Ala12 (β-strand 1); Gln38-Leu44 (β-strand 2); Trp50-Phe54 (β-strand 3); Ser58-Asp62 (β-strand 4); and Leu66-Val69 (β-strand 5). The presence of these strands was also confirmed by: (i) long-distance NOEs involving backbone amides and H$_\alpha$ protons of residues located in the different β-strands (Fig. 2), together with long-distance NOEs of backbone amides or H$_\alpha$ protons with the side-chains of residues located in the different β-strands; and, (ii) consistency between the observed slow-exchanging protons, after 4 h of dissolving the protein in D$_2$O, and the hydrogen-bond scaffolding characteristic of a β-sheet conformation (the green rectangles in Fig. 3) as defined by the structures of CYANA. The hydrogen-bonds observed in at least five out of the final twenty best structures from CYANA (with the lowest target function) defining the β-sheet scaffold are: Val9(NH)-Gly39(CO); Gly39(NH)-Val9(CO); Thr40 (NH)-Leu53(CO); Ile41(NH)-Asp7(CO); Thr42(NH)-Val51(CO); Vale52-Phe59(CO); Leu53(NH)-Thr40(CO); Leu61(NH)-Trp50(CO); and Ser67(NH)-Arg10(CO). Whereas, the turns were defined by the hydrogen-bonds: Arg45(NH)-Gly43(CO); Gly57(NH)-Phe54(CO); and Phe54(NH)-Gly57(CO). The five-stranded β-sheet appeared well-defined among the twenty conformers; the largest differences among the conformers were clustered in the loops, especially the long one joining β-strands 1 and 2 (Fig. 1 A). Residues which appeared to be outliers in the Ramachandran plot were involved in the loop regions or alternatively, close to the termini of the β-strands; for instance, the sole residue which was an outlier in the Ramachandran plot in the twenty calculated conformers is Lys68, at the end of β-strand 5. All the prolines acquired a trans conformation, as also confirmed by the presence of the observed αδ(i, i+1) NOEs (Fig. 3, white squares).

The chemical shifts of some of the protons of residues Leu33, Gly39, Leu44 and Val52 appeared up-field shifted (BMRB 52171). In all cases, this up-field shift was due to the presence of nearby aromatic rings because of the tertiary structure of the protein: Phe54 and Phe59 were close to Leu33 and Val52; Phe54 was close to Gly39; and, Tyr49 and Trp50 were close to Leu44.

3.2. Backbone dynamics of SipA

Backbone ^{15}N relaxation parameters were obtained for 68 (Fig. 4) out of the 78 residues (all amino acids, except the N- and C-terminal ones and the 8 prolines). The R_1 values were relatively uniform through all the sequence with a mean of 2.35 s^{-1} and a standard deviation of 0.51 s^{-1} (Fig. 4 A). The largest value (3.34 ± 0.12 s^{-1}) corresponded to Glu37, at the beginning of β-strand 2. At the N and C termini of the polypeptide chain, we observed a gradual decrease of the values of R_1.

Conversely, the R_2 values showed a larger variation, with a mean of 7.59 s^{-1} and a standard deviation of 1.98 s^{-1} (Fig. 4 B). We also observed a gradual decrease at both termini of the polypeptide chain. The residues with the largest R_2 values (≥10 s^{-1}) were: Arg10 and Glu37, which also had a large R_1 value (see above); both residues were spatially close in the 3D-structure of SipA (Fig. 2). Those high values of the R_2 indicate a large conformational exchange (i.e., in the microsecond-to-millisecond time regime) contribution [16].

The NOE values for all SipA residues were far from the theoretical value of 0.82, expected for an amide proton in a rigid environment at this field strength [16,30], with Val51 (in β-strand 3) having the largest value: 0.73 (Fig. 4C). In fact, the residues with the highest NOE values were those around β-strands 3 and 4, and following them, those involved in the other strands. On the other hand, residues involved in the loops or turns connecting the strands had very small NOE values (Fig. 4C). These findings suggest that SipA had a large mobility in the picosecond-to-nanosecond time regime. It could be thought that those low values of the NOE were due to a fast-conformational exchange reaction, such as a dimer-swapped formation or the presence of dimeric species. However, we can rule out the presence of dimeric species (either swapped or not) by several pieces of evidence. First, size exclusion
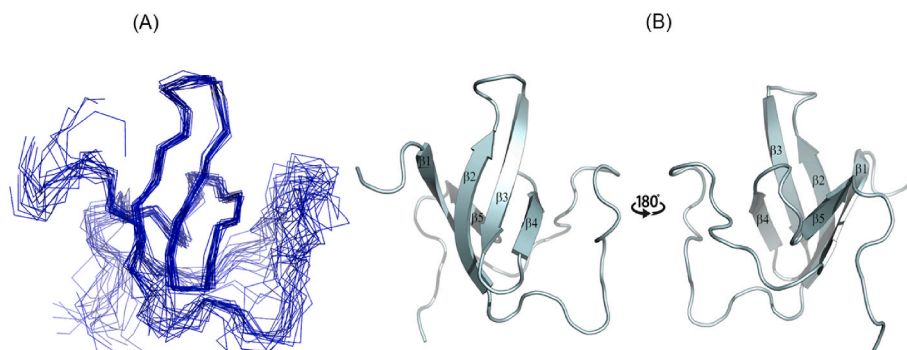
(A) (B)

Fig. 1. Solution structure of isolated SipA. (A) The final twenty NMR conformers of SipA. All conformers are aligned to the first one (with the lowest CYANA target function). (B) Cartoon representation of SipA from two different views. The strands have been labelled. The figures were produced with PyMOL (Schrödinger, USA). The PDB identification number is 8QXI.
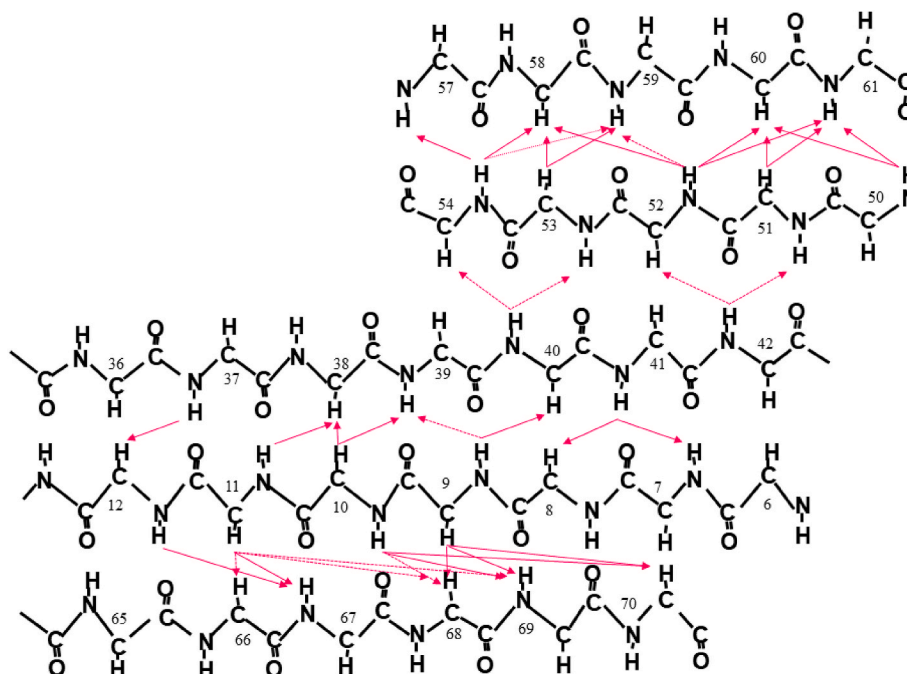

Fig. 2. Scaffolding of the five-stranded β-sheet of SipA. Long-distance NOEs observed in NOESY spectra among the β-strands are shown by continuous arrows. The dotted arrows indicate ambiguous NOEs due to signal overlapping, proximity of the cross-peak to the diagonal, or proximity of the cross-peak to the residual water signal.

chromatography measurements have shown that: (i) SipA has a molecular weight of 7.4 ± 0.8 kDa, close to that obtained from the sequence; and (ii) SipA has a Stokes radius of 14 ± 2 Å, close to that estimated theoretically for a 78-residue-long protein [13,16]. And second, the signals of the protein in the 1D-^{1}H NMR spectrum are very sharp with no evidence of broadening due to conformational exchange (Fig. 1 in Ref. [13]). Then. the low NOE values, even in some of the strands, can be only explained as due to an internal high mobility (we think that this inherent internal high mobility has precluded the crystallization of the protein at the different conditions assayed, MLL-R and AM, unpublished results).

Trying to get insight into the mobility of the residues with large R_2 and small NOE values, we measured the η_{xy} (Fig. 4 D). There was a large variation among the amino acids: the η_{xy} values ranged from 0.695 ± 0.008 s^{-1} for Ser58 (at the N-terminal region of β-strand 4) to 26 ± 7 s^{-1} for Lys19 (at the long loop connecting β-strands 1 and 2). The largest η_{xy} values (>20 s^{-1}) corresponded to residues: Lys19, Leu24, Leu44 and Phe59. As the η_{xy} does not rely on the R_{ex} contribution [20,21], we determined the transversal relaxation rate without any exchange

contribution, R_2^0 (Eq. (2)), and from that value, the conformational exchange term, R_{ex} (Eq. (1)), could be obtained. The R_{ex} determined with this approach was larger (>6.5 s^{-1}) for residues: Ala21 (in the long loop connecting β-strands 1 and 2) and Ser58 (at the N-terminal region of β-strand 4), but there were many residues where the difference between R_2 and R_2^0 was negative (Eq. (1)), which is not physically possible, indicating that the movement of the most of residues occurred in different time regimes [20,21].

Since the small NOE values and the calculations carried out with η_{xy} indicate that SipA had a large mobility in different time scales, we decided to explore further this apparent intrinsic flexibility. We calculated the R_1R_2 product, since high R_1R_2 values reflect the presence of conformational exchange (i.e., in the millisecond-to-second time scale), and low R_1R_2 values monitor fast motions [31]. We determined the $<R_1R_2>$, the trimmed mean value after exclusion of residues with values of NOE <0.1 (Leu24, Ser71 and Ser74), yielding a value of 19.2 s^{-2} (with a standard deviation, σ, of 6.5 s^{-2}). Roughly, half of the residues (35) had values larger than the $<R_1R_2>$ (Fig. S1), whereas the other half (33) had R_1R_2 values below this mean, and thus, they were affected by fast
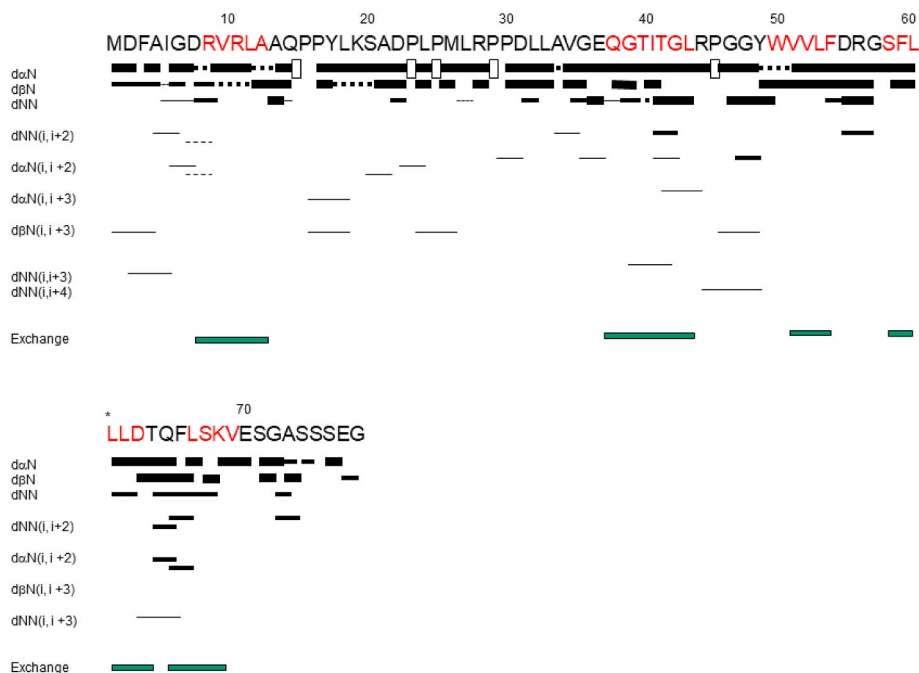
Fig. 3. Summary of NMR data of SipA. NOEs are classified into strong, medium or weak according to the height of the bar underneath the sequence, as concluded from peak integration. Dotted bars indicate NOEs which could not be unambiguously assigned due to signal overlapping or proximity to the residual water signal. The corresponding sequential H_α NOE with the following H_δ of the proline residue are indicated by an open bar in the row corresponding to the αN (i, i+1) NOEs. The green squares at the bottom of the figure indicate those residues that were detected in a 2D ^{1}H–^{15}N HSQC spectrum after 4 h of exchange at pH 5.5 and 25 °C, i.e., solvent-exchange protected residues. The asterisk over the "L" indicates that the Leu symbol (of Leu60) has been repeated to allow for the definition of the NOEs involving this residue. Residues in red in the sequence at the top are those to be involved in β-strands according to TALOS + [26] predictions.
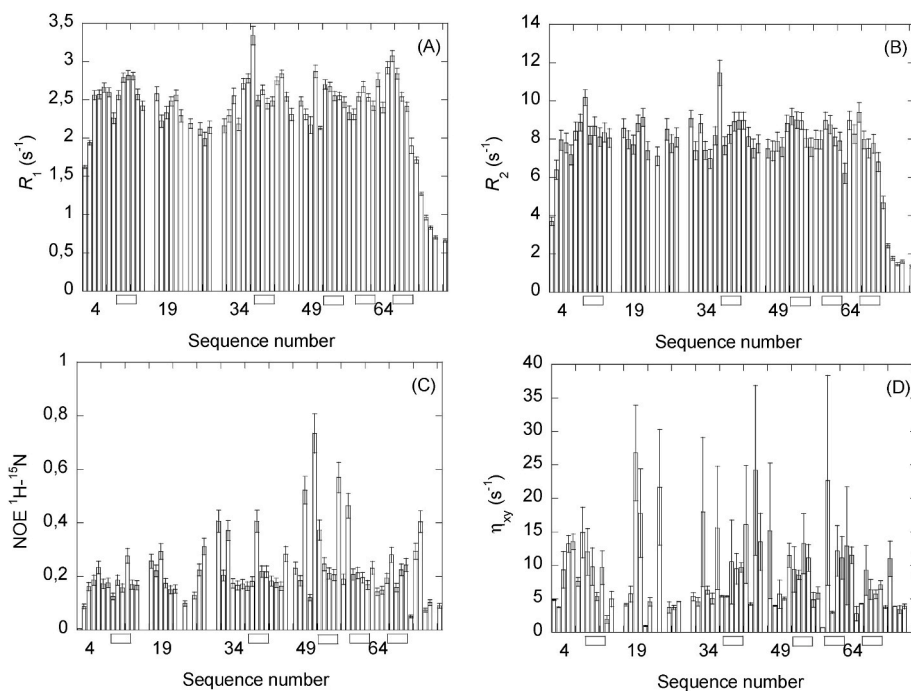

Fig. 4. Relaxation parameters of SipA. The R_1 (A), R_2 (B), NOE (C) and η_{xy} (D) values for residues of SipA acquired at 500 MHz (11.14 T). Error bars in R_1, R_2 and η_{xy} values are from fitting to exponential curves or the hyperbolic tangent. Errors in NOE are estimated to be 10 % of the reported value. The white squares, at the bottom or the graphs, indicate the β-strands according to the structure shown in Fig. 1.

motions. Thus, we can confirm, based solely in the R_1 and R_2 values, that all the residues of SipA had different mobility in a wide range of time-scales. It is important to indicate that we have not used the Lipari-Szabo formalism - where specification of the microscopic motional model is not required - nor, alternatively, the reduced spectral density mapping, where no model is used to define the spectral density function, in our discussion of SipA dynamics to avoid an over-interpretation of the results. However, we can try to sharpen the discussion of our results, to
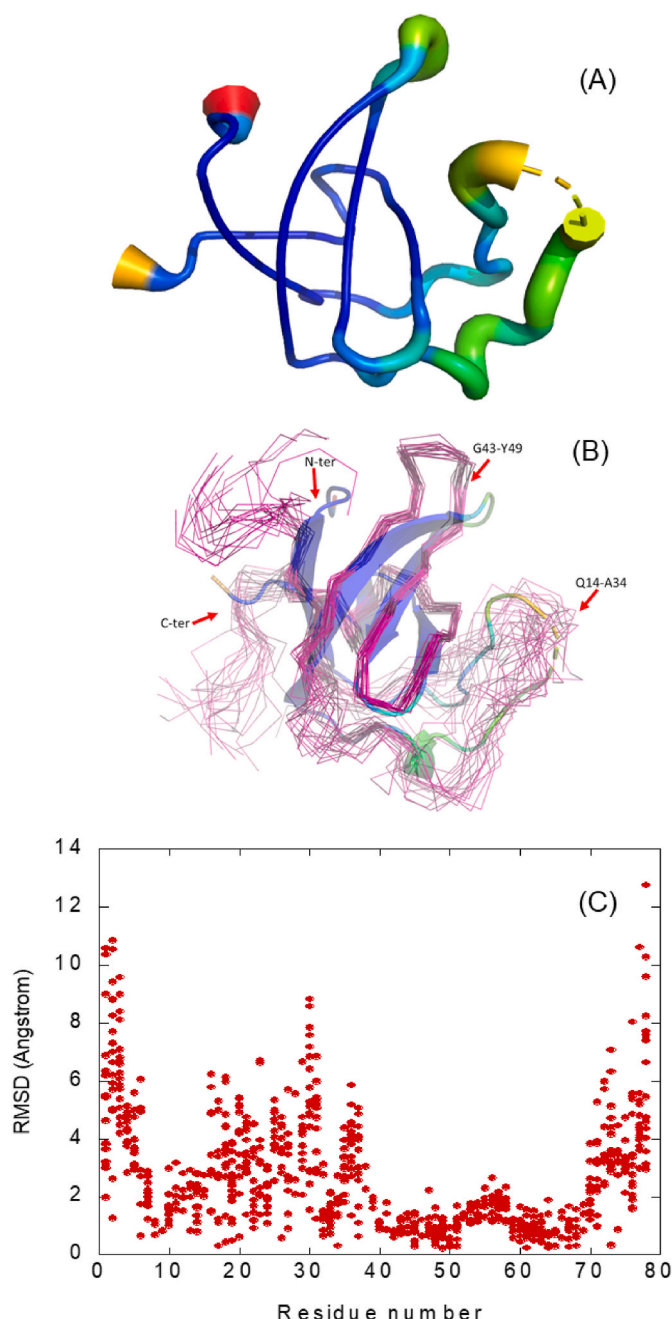
Fig. 5. Comparison of NMR structure with an AlphaFold model of SipA. (A) Model of SipA obtained with Phenix 1.21rc1.5109. Regions with low plDDT appear in red (plDDT 50–60), yellow (plDDT 70–80) or in green colors (plDDT 80–90) (depending on the value of plDDT parameter). Residues Met1, Pro23-Pro25 and Ser71-Gly78 were removed from the processed AlphaFold model because the low plDDT parameters. Those well-defined regions appear in blue (plDDT >90). (B) Superposition of the AF_model (blue) with the 20 structures from NMR (light magenta). The regions with a low plDDT, and a high RMSD as shown in panel B are indicated with red arrows. (C) Representation of the RMSD values *per* residue of the 20 NMR conformers; not all residues are represented for each of the conformers to avoid overcrowding in the plot.

provide a number which could also pinpoint to the high mobility of SipA, by using the S^2 parameter from the Lipari-Szabo formalism. The S^2 parameter is the square of the generalized order parameter that characterizes the amplitude of the intramolecular motion in a molecular reference frame; it satisfies the inequality $0 \leq S^2 \leq 1$, in which lower values indicate larger amplitudes of internal motions, and the limit

value, $S^2 = 0$, corresponds to the movement of the N–H vector isotropically through all possible orientations relative to the rest of the molecule. Thus, although we do not apply the Lipari-Szabo model in depth, we can provide an estimation of an averaged S^2, to further discuss on the mobility of SipA. Then, we used the R_1R_2 product to estimate the averaged generalized order parameter, S^2_{av}, given by: $S^2_{av} = \sqrt{<R_1R_2>/R_1R_2{}^{max}}$, where $R_1R_2{}^{max}$ is the maximum value (that of Glu37, with a value of 38.27 s^{-2}). This equation yielded a S^2_{av} of 0.708, which further confirms that SipA is a highly flexible protein, because this value is much smaller than that theoretically predicted in a rigid protein of this size (0.82) [16,30].

An estimation of the correlation time of 3.2 ± 0.5 ns, where 0.5 is the standard deviation, was obtained from a trimmed R_2/R_1 (excluding those residues indicated above with very low NOE values) [30]. This value of the correlation time is within the error of that determined previously based on homonuclear echo-*anti*-echo T_2-relaxation time measurements [13], which was 3.7 ns. This agreement indicates the robustness of our measurements and pinpoints to the inherent high mobility of SipA [32–35].

3.3. Analysis and comparison of the SipA structure determined by NMR with that predicted by AlphaFold

It is important to indicate that there is no structure of SipA in the PDB [36], or that of any homologous protein (in Uniprot database). In fact, a BLAST [37–39] search both in PDB and Uniprot did not produce any homologous structure. However, searching in the database of non-redundant protein sequences, BLAST yielded several structures with domains of unknown function (DUFs). That is why to make a model to compare with our experimentally-determined structure, we used AlphaFold [28,40]. Indeed, the main differences between the 20 conformers and the AF_model were found in these regions of lower plDDT values in the AF_model (Fig. 5 A, B). These residues of low confidence belong to the N and C termini of the protein; those amino acids intervening in the long loop region connecting β-strands 1 and 2 (Asp22-Met26), which involves two prolines (Pro23 and Pro25) (both regions have been indicated in the figure, as they belong to the polypeptide patch Gln14-Ala34); and the region Gly43-Tyr49 (Fig. 5C). The regions with low plDDT values agree with those having a high RMSD *per* residue in the 20 conformers (Fig. 5C), and where more differences are observed among the 20 conformers and the AF_ Model (Fig. 5 B, C). In fact, it has been suggested that the regions with low plDDT values can be correlated to different existing conformations in the protein structure [41]. As expected, residues in the β-strands (i.e., the region around Val51, forming β-strand 3) showed the lower RMSD *per* residue values between the solution structure determined by NMR. On the other hand, those amino acids belonging to β-strand 5, close to the C-terminal region of SipA showed also large RMSD *per* residue values (Fig. 5C).

We also carried out a DALI search firstly with the models from the whole PDB, and secondly with the models from the AlphaFold [28,40] database, as DALI can identify related structures, even with modest sequence identity. The results with the whole PDB yielded 334 polypeptide chains, with a sequence similarity with SipA between 6 and 18 %. The most abundant class of proteins are tyrosine protein kinases and SH3-domain-containing proteins. On the other hand, the search with the AlphaFold database led to 61 polypeptide chains, with a percentage of sequence identity with SipA between 9 and 23 %. In this case, the most abundant class of proteins, whose structure have some similarity to that of SipA, corresponds to E3-ubiquitin protein ligases, although there were also several kinases and SH3-domain-containing proteins.

4. Discussion

We have solved the structure of the small regulatory factor SipA in solution. Our results show that the structure was formed by five

β-strands arranged in an antiparallel way; this structure was reminiscent of β-class II proteins. Comparison of a constructed AlphaFold model with our structure suggests that both were nearly identical except for differences in the loops connecting the different β-strands (as it happens among the twenty conformers from NMR calculations).

The comparison of the dynamics in the time scales provided by solvent-exchange (millisecond-to-second time regime) (Fig. 3, green squares) with that provided by the relaxation measurements (picosecond-to-nanosecond time regime) (Fig. 4) indicate that residues with slow solvent-exchange were those with a larger NOE value (around Val51, forming the inner region of the protein). Thus, exchange at those sites should take place during global unfolding events, where residues have a reduced mobility in the picosecond-to-nanosecond time regime. Also, there were flexible regions of SipA with movements in the millisecond-to-second time regime, as judged by the large values of R_2 (Fig. 4 B) and the calculation of R_{ex} from η_{xy}. Therefore, it seems that residues of SipA were affected by a large flexibility, having conformational movements in different time scales independently of the type of secondary structure. However, it is important to pinpoint that residues in the loops or turns appeared to have movements in a wider range of times scales than those in the strands (ordered structure).

Small proteins appear to play critical roles in key cyanobacterial processes such photosynthesis or regulation of the carbon to nitrogen balance [3,42]. A paradigmatic example is the inhibition by nitrogen abundance of glutamine synthetase function, executed by two small proteins instead of by covalent modification, which is the main mechanism in proteobacteria [43–46]. Recent work in *Synecocystis* sp. PCC 6803 [44,47,48] has shown that small proteins (called Pir proteins for PII-interacting regulators) exert key regulatory roles in the context of carbon-to-nitrogen balance by binding to the essential nitrogen regulator PII. SipA could be one of those small proteins playing key functions (still unknown in this case) in cyanobacteria.

Flexibility in proteins is required to achieve a proper function, often encompassing huge networks of evolutionarily conserved clusters of residues spanning an entire protein domain [49,50]. For SipA, this functional feature could be a key requirement for recognition and binding to NblS (as far the sole known function of SipA, and that is why it is classified as a DUF), its biological partner [4,5]; this binding may be facilitated by the flexibility of the connecting loops and the ends of the β-strands from which they emerge. In SipA, probably the N terminus of β-strand 2, around Glu37, which has large values of R_1 and R_2 rates, might act as a picosecond-to-nanosecond hinge for the opening of this strand, weakening the whole scaffold of the sheet, when bound to NblS. The movements of other regions of the protein will not have to involve large amplitude collective motions, but they probably implicate small amplitude fast fluctuations occurring very often. We hypothesize that Glu37 is probably involved in binding to NblS, and we shall explore this hypothesis in future works, now the structure of SipA is known.

Finally, it is important to indicate that the flexibility described in this work explains another important future of SipA. This increase in flexibility exhibited at different time scales would result in an increase in protein stability, as we have previously shown by using fluorescence and CD in the presence of denaturants and with heat [13]. GdmCl (guanidinium chloride)-chemical denaturation of SipA is not a two-state process, showing different midpoints when it is followed by fluorescence or far-UV CD. The same happens (i.e. a non-two-state process) when unfolding is followed by thermal denaturations, with thermal denaturation midpoints different between fluorescence and far-UV CD. By considering the values of the enthalpy, the thermal denaturation midpoint and the heat capacity previously measured from fluorescence, the apparent free energy of denaturation, ΔG, at 298 K was 11.4 kcal mol^{-1} [13], which is high for such a small protein like SipA. However, this high value can be rationalized by the high mobility observed in this work, since the inherent flexibility of the protein favors the folded state by raising its entropy.

Supplementary material

There is one figure showing the R_1R_2 plot (Fig. S1). There is a table showing the complete suite of NMR experiment used during SipA assignment.

Authors' contributions

Conceptualization, JLN, MLLR, AM, AC and ACA; methodology, JLN, and ACA; investigation, JLN, and ACA; data formal analysis, JLN; writing-original draft preparation, JLN and ACA; materials, JLN, AC, MLLA, AM and ACA; writing-review and editing, JLN, AC, MLLA, AM and ACA; funding acquisition, AC, AM, JLN and ACA.

All authors have read and agreed to the published version of the manuscript.

Data availability

The datasets generated during and/or analyzed during the current study are available from the corresponding authors on reasonable request.

Deposition

The chemical shifts of SipA (^{13}C, ^{15}N and ^{1}H) have been deposited in the BMRB under the accession number 52171. The 20 conformers with the lowest target function have been deposited in the PDB, together with the list of restrictions (distances and angles) used, under the identification number 8QXI.

CRediT authorship contribution statement

José L. Neira: Writing – review & editing, Writing – original draft, Visualization, Validation, Resources, Project administration, Methodology, Investigation, Funding acquisition, Formal analysis, Conceptualization. **María Luisa López-Redondo:** Writing – review & editing, Writing – original draft, Resources. **Ana Cámara-Artigas:** Writing – review & editing, Writing – original draft, Validation, Methodology, Investigation, Formal analysis, Conceptualization. **Alberto Marina:** Writing – review & editing, Writing – original draft, Resources, Funding acquisition. **Asunción Contreras:** Writing – review & editing, Writing – original draft, Resources, Funding acquisition.

Declaration of competing interest

The authors have no relevant financial or non-financial interest to disclosure.

Appendix A. Supplementary data

Supplementary data to this article can be found online at https://doi.org/10.1016/j.abb.2024.109943.

References

[1] A.R. Grossman, M.R. Schaefer, G.G. Chiang, J.L. Collier, The phycobilisome, a light-harvesting complex responsive to environmental conditions, Microbiol. Rev. 57 (1993) 725–749, https://doi.org/10.1128/MR.57.3.725-749.1993.

[2] R. Groben, D. Kaloudas, C.A. Raines, B. Offmann, S.C. Maberly, B. Gontero, Comparative sequence analysis of CP12, a small protein involved in the formation of a Calvin cycle complex in photosynthetic organisms, Photosynth. Res. 103 (2010) 183–194, https://doi.org/10.1007/S11120-010-9542-Z/TABLES/2.

[3] G. Storz, Y.I. Wolf, K.S. Ramamurthi, in: Small Proteins Can No Longer Be Ignored, vol. 83, 2014, pp. 753–777, https://doi.org/10.1146/ANNUREV-BIOCHEM-070611-102400, 10.1146/Annurev-Biochem-070611-102400.

[4] J. Espinosa, I. Fuentes, S. Burillo, F. Rodríguez-Mateos, A. Contreras, SipA, a novel type of protein from Synechococcus sp. PCC 7942, binds to the kinase domain of NblS, FEMS Microbiol. Lett. 254 (2006) 41–47, https://doi.org/10.1111/J.1574-6968.2005.00007.X.

[5] P. Salinas, D. Ruiz, R. Cantos, M.L. Lopez-Redondo, A. Marina, A. Contreras, The regulatory factor SipA provides a link between NblS and NblR signal transduction pathways in the cyanobacterium Synechococcus sp. PCC 7942, Mol. Microbiol. 66 (2007) 1607–1619, https://doi.org/10.1111/J.1365-2958.2007.06035.X.

[6] T. Sakayori, Y. Shiraiwa, I. Suzuki, A Synechocystis homolog of SipA protein, Ssl3451, enhances the activity of the histidine kinase Hik33, Plant Cell Physiol. 50 (2009) 1439–1448, https://doi.org/10.1093/PCP/PCP089.

[7] M.L. López-Redondo, F. Moronta, P. Salinas, J. Espinosa, R. Cantos, R. Dixon, A. Marina, A. Contreras, Environmental control of phosphorylation pathways in a branched two-component system, Mol. Microbiol. 78 (2010) 475–489, https://doi.org/10.1111/J.1365-2958.2010.07348.X.

[8] M.K. Ashby, C.W. Mullineaux, Cyanobacterial ycf27 gene products regulate energy transfer from phycobilisomes to photosystems I and II, FEMS Microbiol. Lett. 181 (1999) 253–260, https://doi.org/10.1111/J.1574-6968.1999.TB08852.X.

[9] F. Moronta-Barrios, J. Espinosa, A. Contreras, Negative control of cell size in the cyanobacterium Synechococcus elongatus PCC 7942 by the essential response regulator RpaB, FEBS Lett. 587 (2013) 504–509, https://doi.org/10.1016/J.FEBSLET.2013.01.023.

[10] J. Espinosa, J.S. Boyd, R. Cantos, P. Salinas, S.S. Golden, A. Contreras, Cross-talk and regulatory interactions between the essential response regulator RpaB and cyanobacterial circadian clock output, Proc. Natl. Acad. Sci. U. S. A. 112 (2015) 2198–2203, https://doi.org/10.1073/PNAS.1424632112/SUPPL_FILE/PNAS.201424632SI.PDF.

[11] M. Riediger, Y. Hihara, W.R. Hess, From cyanobacteria and algae to land plants: the RpaB/Ycf27 regulatory network in transition, Perspect. Phycol. 5 (2018) 13–25, https://doi.org/10.1127/PIP/2018/0078.

[12] P. Casino, V. Rubio, A. Marina, Structural insight into partner specificity and phosphoryl transfer in two-component signal transduction, Cell 139 (2009) 325–336, https://doi.org/10.1016/J.CELL.2009.08.032.

[13] M.L. López-Redondo, A. Contreras, A. Marina, J.L. Neira, The regulatory factor SipA is a highly stable beta-II class protein with a SH3 fold, FEBS Lett. 584 (2010) 989–994, https://doi.org/10.1016/J.FEBSLET.2010.01.043.

[14] P.G. Blommel, B.G. Fox, A combined approach to improving large-scale production of tobacco etch virus protease, Protein Expr. Purif. 55 (2007) 53–68, https://doi.org/10.1016/J.PEP.2007.04.013.

[15] S.C. Gill, P.H. von Hippel, Calculation of protein extinction coefficients from amino acid sequence data, Anal. Biochem. 182 (1989) 319–326, https://doi.org/10.1016/0003-2697(89)90602-7.

[16] J. Cavanagh, W.J. Fairbrother, A.G. Palmer, N.J. Skelton, Protein NMR Spectroscopy: Principles and Practice, second ed., 2007.

[17] D. Pantoja-Uceda, J. Santoro, Amino acid type identification in NMR spectra of proteins via beta- and gamma-carbon edited experiments, J. Magn. Reson. 195 (2008) 187–195, https://doi.org/10.1016/J.JMR.2008.09.010.

[18] D. Pantoja-Uceda, J. Santoro, New amino acid residue type identification experiments valid for protonated and deuterated proteins, J. Biomol. NMR 54 (2012) 145–153, https://doi.org/10.1007/S10858-012-9665-Y.

[19] N.A. Farrow, R. Muhandiram, S.M. Pascal, L.E. Kay, A.U. Singer, J.D. Forman-Kay, C.M. Kay, G. Gish, T. Pawson, S.E. Shoelson, Backbone dynamics of a free and phosphopeptide-complexed Src homology 2 domain studied by 15N NMR relaxation, Biochemistry 33 (1994) 5984–6003, https://doi.org/10.1021/BI00185A040.

[20] N. Tjandra, P. Wingfield, S. Stahl, A. Bax, Anisotropic rotational diffusion of perdeuterated HIV protease from 15N NMR relaxation measurements at two magnetic fields, J. Biomol. NMR 8 (1996) 273–284, https://doi.org/10.1007/BF00410326.

[21] N. Rezaei-Ghaleh, K. Giller, S. Becker, M. Zweckstetter, Effect of zinc binding on β-amyloid structure and dynamics: implications for Aβ aggregation, Biophys. J. 101 (2011) 1202–1211, https://doi.org/10.1016/J.BPJ.2011.06.062.

[22] W. Lee, M. Tonelli, J.L. Markley, NMRFAM-SPARKY: enhanced software for biomolecular NMR spectroscopy, Bioinformatics 31 (2015) 1325–1327, https://doi.org/10.1093/BIOINFORMATICS/BTU830.

[23] T. Herrmann, P. Güntert, K. Wüthrich, Protein NMR structure determination with automated NOE assignment using the new software CANDID and the torsion angle dynamics algorithm DYANA, J. Mol. Biol. 319 (2002) 209–227, https://doi.org/10.1016/S0022-2836(02)00241-3.

[24] P. Güntert, C. Mumenthaler, K. Wüthrich, Torsion angle dynamics for NMR structure calculation with the new program DYANA, J. Mol. Biol. 273 (1997) 283–298, https://doi.org/10.1006/JMBI.1997.1284.

[25] P. Güntert, W. Braun, K. Wüthrich, Efficient computation of three-dimensional protein structures in solution from nuclear magnetic resonance data using the program DIANA and the supporting programs CALIBA, HABAS and GLOMSA, J. Mol. Biol. 217 (1991) 517–530, https://doi.org/10.1016/0022-2836(91)90754-T.

[26] Y. Shen, F. Delaglio, G. Cornilescu, A. Bax, TALOS+: a hybrid method for predicting protein backbone torsion angles from NMR chemical shifts, J. Biomol. NMR 44 (2009) 213–223, https://doi.org/10.1007/S10858-009-9333-Z.

[27] A. Bhattacharya, R. Tejero, G.T. Montelione, Evaluating protein structures determined by structural genomics consortia, Proteins 66 (2007) 778–795, https://doi.org/10.1002/PROT.21165.

[28] R.D. Oeffner, T.I. Croll, C. Millán, B.K. Poon, C.J. Schlicksup, R.J. Read, T.C. Terwilliger, Putting AlphaFold models to work with phenix.process_predicted_model and ISOLDE, Acta Crystallogr D Struct Biol 78 (2022) 1303–1314, https://doi.org/10.1107/S2059798322010026/AI5009SUP8.MP4.

[29] L. Willard, A. Ranjan, H. Zhang, H. Monzavi, R.F. Boyko, B.D. Sykes, D.S. Wishart, VADAR: a web server for quantitative evaluation of protein structure quality, Nucleic Acids Res. 31 (2003) 3316–3319, https://doi.org/10.1093/NAR/GKG565.

[30] L.E. Kay, D.A. Torchia, A. Bax, Backbone dynamics of proteins as studied by 15N inverse detected heteronuclear NMR spectroscopy: application to staphylococcal nuclease, Biochemistry 28 (1989) 8972–8979, https://doi.org/10.1021/BI00449A003.

[31] J.M. Kneller, M. Lu, C. Bracken, An effective method for the discrimination of motional anisotropy and chemical exchange, J. Am. Chem. Soc. 124 (2002) 1852–1853, https://doi.org/10.1021/JA017461K.

[32] J.H. Viles, D. Donne, G. Kroon, S.B. Prusiner, F.E. Cohen, H.J. Dyson, P.E. Wright, Local structural plasticity of the prion protein. Analysis of NMR relaxation dynamics, Biochemistry 40 (2001) 2743–2753, https://doi.org/10.1021/BI002898A.

[33] V.A. Jarymowycz, M.J. Stone, Fast time scale dynamics of protein backbones: NMR relaxation methods, applications, and functional consequences, Chem. Rev. 106 (2006) 1624–1671, https://doi.org/10.1021/CR040421P.

[34] G.M. Clore, P.C. Driscoll, A.M. Gronenborn, P.T. Wingfield, Analysis of the backbone dynamics of interleukin-1 beta using two-dimensional inverse detected heteronuclear 15N-1H NMR spectroscopy, Biochemistry 29 (1990) 7387–7401, https://doi.org/10.1021/BI00484A006.

[35] C.P.M. Van Mierlo, N.J. Darby, J. Keeler, D. Neuhaus, T.E. Creighton, Partially folded conformation of the (30-51) intermediate in the disulphide folding pathway of bovine pancreatic trypsin inhibitor. 1H and 15N resonance assignments and determination of backbone dynamics from 15N relaxation measurements, J. Mol. Biol. 229 (1993) 1125–1146, https://doi.org/10.1006/JMBI.1993.1108.

[36] H. Berman, K. Henrick, H. Nakamura, Announcing the worldwide protein data bank, Nat. Struct. Biol. 10 (2003) 980, https://doi.org/10.1038/NSB1203-980.

[37] S.F. Altschul, T.L. Madden, A.A. Schäffer, J. Zhang, Z. Zhang, W. Miller, D.J. Lipman, Gapped BLAST and PSI-BLAST: a new generation of protein database search programs, Nucleic Acids Res. 25 (1997) 3389–3402, https://doi.org/10.1093/NAR/25.17.3389.

[38] C. Camacho, G. Coulouris, V. Avagyan, N. Ma, J. Papadopoulos, K. Bealer, T.L. Madden, BLAST+: architecture and applications, BMC Bioinf. 10 (2009), https://doi.org/10.1186/1471-2105-10-421.

[39] S.F. Altschul, W. Gish, W. Miller, E.W. Myers, D.J. Lipman, Basic local alignment search tool, J. Mol. Biol. 215 (1990) 403–410, https://doi.org/10.1016/S0022-2836(05)80360-2.

[40] M. Akdel, D.E.V. Pires, E.P. Pardo, J. Jänes, A.O. Zalevsky, B. Mészáros, P. Bryant, L.L. Good, R.A. Laskowski, G. Pozzati, A. Shenoy, W. Zhu, P. Kundrotas, V.R. Serra, C.H.M. Rodrigues, A.S. Dunham, D. Burke, N. Borkakoti, S. Velankar, A. Frost, J. Basquin, K. Lindorff-Larsen, A. Bateman, A.V. Kajava, A. Valencia, S. Ovchinnikov, J. Durairaj, D.B. Ascher, J.M. Thornton, N.E. Davey, A. Stein, A. Elofsson, T.I. Croll, P. Beltrao, A structural biology community assessment of AlphaFold2 applications, Nat. Struct. Mol. Biol. 29 (2022) 1056–1067, https://doi.org/10.1038/S41594-022-00849-W.

[41] T. Saldaño, N. Escobedo, J. Marchetti, D.J. Zea, J. Mac Donagh, A.J. Velez Rueda, E. Gonik, A. Garciá Melani, J. Novomisky Nechcoff, M.N. Salas, T. Peters, N. Demitroff, S. Fernandez Alberti, N. Palopoli, M.S. Fornasari, G. Parisi, Impact of protein conformational diversity on AlphaFold predictions, Bioinformatics 38 (2022) 2742–2748, https://doi.org/10.1093/BIOINFORMATICS/BTAC202.

[42] F. Brandenburg, S. Klähn, Small but smart: on the diverse role of small proteins in the regulation of cyanobacterial metabolism, Life 10 (2020) 322, https://doi.org/10.3390/LIFE10120322, 2020.

[43] M. García-Domínguez, J.C. Reyes, F.J. Florencio, Glutamine synthetase inactivation by protein-protein interaction, Proc. Natl. Acad. Sci. U. S. A. 96 (1999) 7161–7166, 10.1073/PNAS.96.13.7161/ASSET/1F1393CD-3965-418D-8BCC-7842A65680F1/ASSETS/GRAPHIC/PQ1390665005.JPEG.

[44] A. Herrero, A.M. Muro-Pastor, E. Flores, Nitrogen control in cyanobacteria, J. Bacteriol. 183 (2001) 411–425, https://doi.org/10.1128/JB.183.2.411-425.2001.

[45] S. Klähn, C. Schaal, J. Georg, D. Baumgartner, G. Knippen, M. Hagemann, A.M. Muro-Pastor, W.R. Hess, The sRNA NsiR4 is involved in nitrogen assimilation control in cyanobacteria by targeting glutamine synthetase inactivating factor IF7, Proc. Natl. Acad. Sci. U. S. A. 112 (2015) E6243, https://doi.org/10.1073/PNAS.1508412112/SUPPL_FILE/PNAS.1508412112.SAPP.PDF. –E6252.

[46] J.C. Reyes, F.J. Florencio, A novel mechanism of glutamine synthetase inactivation by ammonium in the cyanobacterium Synechocystis sp. PCC 6803. Involvement of an inactivating protein, FEBS Lett. 367 (1995) 45–48, https://doi.org/10.1016/0014-5793(95)00544-J.

[47] P. Bolay, R. Rozbeh, M. Isabel Muro-Pastor, S. Timm, M. Hagemann, F.J. Florencio, K. Forchhammer, S. Klähn, The novel PII-interacting protein PirA controls flux into the cyanobacterial ornithine-ammonia cycle, mBio 12 (2021), https://doi.org/10.1128/MBIO.00229-21.

[48] T. Orthwein, J. Scholl, P. Spät, S. Lucius, M. Koch, B. Macek, M. Hagemann, K. Forchhammer, The novel PII-interactor PirC identifies phosphoglycerate mutase as key control point of carbon storage metabolism in cyanobacteria, Proc. Natl.

Acad. Sci. U. S. A. 118 (2021) e2019988118, https://doi.org/10.1073/PNAS.2019988118/SUPPL_FILE/PNAS.2019988118.SAPP.PDF.

[49] G.P.P. Lisi, G.A.A. Manley, H. Hendrickson, I. Rivalta, V.S.S. Batista, J.P. Loria, Dissecting dynamic allosteric pathways using chemically related small-molecule activators, Structure 24 (2016) 1155–1166, https://doi.org/10.1016/J.STR.2016.04.010.

[50] G.S. Kumar, M.W. Clarkson, M.B.A. Kunze, D. Granata, A. Joshua Wand, K. Lindorff-Larsen, R. Page, W. Peti, Dynamic activation and regulation of the mitogen-activated protein kinase p38, Proc. Natl. Acad. Sci. U. S. A. 115 (2018) 4655–4660, https://doi.org/10.1073/PNAS.1721441115/-/DCSUPPLEMENTAL.